Clarity analysis of the Cl/pH sensor expression in the brain of transgenic mice

Artem V Diuba, Dmitry Samigullin, Attila Kaszas, Francesca Zonfrillo, Anton Malkov, Elena Petukhova, Antonio Casini, Daniele Arosio, Monique Esclapez, Cornelius T Gross, et al.

Clarity analysis of the Cl/pH sensor expression in the brain of transgenic mice.

Artem V. Diuba[1,2], Dmitry V. Samigullin [3,4,5], Attila Kaszas[1,11], Francesca Zonfrillo[6], Anton Malkov[1,7], Elena Petukhova[8], Antonio Casini[9], Daniele Arosio[10], Monique Esclapez[1], Cornelius T. Gross[6], Piotr Bregestovski[1,8,*]

[1]Aix-Marseille University, INSERM, INS, Institut of System Neurosciences, 13005 Marseille, France;
[2]A.N. Belozersky Institute of Physico-Chemical Biology, M.V. Lomonosov Moscow State University, 119992, Moscow, Russia;
[3] Laboratory of Biophysics of Synaptic Processes, Kazan Institute of Biochemistry and Biophysics, FRC Kazan Scientific Center of RAS, 420111, Kazan, Russia;
[4] Department of Radiophotonics and microwave technologies, Kazan National Research Technical University named after A.N.Tupolev, 420111, Kazan, Russia;
[5] Open Laboratory of Neuropharmacology, Kazan Federal University,420111, Kazan, Russia,
[6]Epigenetics and Neurobiology Unit, European Molecular Biology Laboratory, EMBL-Rome, Via Ramarini 32, 00015 Monterotondo, ITALY;
[7]Institute of Theoretical and Experimental Biophysics, Russian Academy of Sciences, 142290, Pushchino, Russia;
[8]Institute of Neurosciences, Kazan Medical State University, Kazan, Russia
[9]CIBIO University of Trento, Italy
[10]Institute of Biophysics, National Research Council of Italy, 38123 Trento, Italy;
[11]Institut de Neurosciences de la Timone, CNRS UMR 7289 & Aix- Marseille Université, 13005 Marseille, France

[*]Correspondence to P. Bregestovski: e-mails: piotr.bregestovski@univ-amu.fr
pbreges@gmail.com

Running title: ClopHensor distribution in transgenic mice

Abbreviations: aCSF - artificial cerebrospinal fluid; Cl^- - chloride; $[Cl^-]_i$ - intracellular chloride concentration; GFP - green fluorescent protein; LAL - *levator auris longus* nerve–muscle preparation; PBST- Phosphate buffered saline with Tween-20; PFA - paraformaldehyde.

ABSTRACT

Genetically encoded biosensors are widely used in cell biology for the non-invasive imaging of concentrations of ions or the activity of enzymes, to evaluate the distribution of small molecules, proteins and organelles, and to image protein interactions in living cells. These fluorescent molecules can be used either by transient expression in cultured cells or in entire organisms or through stable expression by producing transgenic animals characterized by genetically encoded and heritable biosensors. Using the mouse Thy1 mini-promoter, we generated a line of transgenic mice expressing a genetically encoded sensor for the simultaneous measurements of intracellular Cl^- and pH. This construct, called ClopHensor, consists of a H^+- and Cl^--sensitive variant of the enhanced green fluorescent protein (E^2GFP) fused with a red fluorescent protein (DsRedm). Stimulation of hippocampal Schaffer collaterals proved that the sensor is functionally active. To reveal the expression pattern of ClopHensor across the brain of transgenic mice, we obtained transparent brain samples using the CLARITY method and imaged them with confocal and light-sheet microscopy. We then developed a semi-quantitative approach to identify brain structures with high intrinsic sensor fluorescence. This approach allowed us to assess cell morphology and track axonal projection, as well as to confirm E^2GFP and DsRedm fluorescence colocalization. This analysis also provides a map of the brain areas suitable for non-invasive monitoring of intracellular Cl^-/pH in normal and pathological conditions.

Keywords: genetically encoded biosensors; intracellular ions monitoring; fluorescence imaging.

INTRODUCTION

Chloride (Cl^-), the most abundant physiological anion, is present in every cell and participates in a variety of physiological functions, including neurotransmission, regulation of cell volume and intracellular pH, fluid secretion and stabilisation of resting membrane potential (Aslanova et al., 2006; Pasantes-Morales et al., 2006; Suzuki et al., 2006). The concentration of intracellular Cl^- ($[Cl^-]_i$) and its cellular permeability are tightly regulated by a variety of Cl^--selective channels and Cl^- transporters (Jentsch et al., 2002).

Direct measurement of $[Cl^-]_i$ in neurons and in other cell types is a challenging task owing to two main difficulties: (i) the low transmembrane ratio for Cl^-, approximately 10:1, while, for instance, for Ca^{2+} this ratio is 10000:1; and (ii) a small driving force for Cl^-, as Cl^- reversal potential is usually close to the resting potential of the cell. Consequently, sensitive probes with high dynamic range at physiological $[Cl^-]_i$ are necessary for the reliable analysis of Cl^- distribution and its functional variations. Among the numerous methods for $[Cl^-]_i$ monitoring, genetically encoded probes are the most promising tool for the analysis of Cl^- homeostasis in various cell types, especially in neurons and their processes (rev. Bregestovski et al., 2009; Bregestovski and Arosio, 2012; Arosio and Ratto, 2014).

Several genetically encoded indicators, based on GFP derivatives have been proposed (Kuner and Augustine, 2000; Markova et al., 2008; Waseem et al., 2010; Arosio et al., 2010). The interpretation of the fluorescence signals recorded with these indicators may be complicated by two main factors: (i) variations in $[Cl^-]_i$ are usually accompanied by changes in pH and (ii) most of Cl-sensitive GFP derivatives are also pH-sensitive.

This task was elegantly solved by introducing a new sensor allowing simultaneous measurements of $[Cl^-]_i$ and pH_i local changes (Arosio et al., 2010). This sensor, named ClopHensor, consists of E^2GFP variant fused through 24 amino acid linker with the red fluorescent protein DsRedm. ClopHensor spectral changes are ideally suited for ratiometric imaging at three excitation wavelengths: 458, 488 and 560 nm and this construct demonstrated high stability to bleaching during long fluorescence measurements (Mukhtarov et al., 2013).

To use ClopHensor in defined subsets of neurons, we produced transgenic mice using a strong neuron-specific promoter, Thy1 (Caroni, 1997; Feng et al., 2000). The Thy1 promoter has been successfully used previously to drive the expression of Cl^- indicators in different regions of the brain (Berglund et al., 2006; Batti et al., 2013). Previously, Feng et al. (2000) demonstrated that among 25 independently generated *Thy1-derived* transgenic lines, all of them exhibited a unique heritable pattern of fluorescent protein expression. Also, a recent study on 18 lines demonstrated that some brain areas, like the anterior lateral motor cortex, the primary motor cortex, the hippocampus, the primary somatosensory and visual cortex reveal similar presence of the genetically encoded calcium indicators, while for the other regions a large variability in the expression has been described (Dana et al., 2018). This indicates that for each new Thy1-derived line, a careful analysis of fluorescent protein expression is necessary.

We thus used a well-described tissue-clearing technique, the CLARITY method (Chung and Deisseroth, 2013; Tomer et al., 2014; Stefaniuk et al., 2016) to obtain transparent brain samples and imaged them with confocal and light-sheet microscopy. Finally, based on the acquired expression map, we chose the pyramidal layer of the hippocampal CA1 area - a brain region abundant in ClopHensor-expressing neurons – to prove that the expressed sensor is functionally viable. Our experiments with fluorescent microscopy show functional responses of the sensor, proving that neurons show the expected fluorescence responses to activity changes.

MATERIALS AND METHODS

Generation of Transgenic Mice

Our mice are generated using the Thy1 neuronal promoter (Caroni, 1997) following the strategy used earlier (Batti et al. 2013). ClopHensor cDNA was PCR-amplified from a ClopHensor expression vector (Arosio et al., 2010) and cloned into the XhoI site of the mouse Thy1.2 expression cassette (Caroni, 1997). Linearized, vector-free insert was prepared for pronuclear injection into C57BL/6J × DBA zygotes by agarose gel purification. Two founders carrying the transgene were identified and genotyped by PCR using the following primers: Thy1 forward 5'-TCTGAGTGGCAAAGGACCTTAGG -3' and ClopHensor linker reverse 5'-TCCACGTGGAACTAGACCACC -3'.

The ClopHensor cassette consisted of the following individual sequence elements: a cytomegalovirus-immediate early (CMV-IE) promoter and a chicken beta-actin promoter (CAG); the adenovirus splice donor (SD) and splice acceptor (SA) site from plasmid pSAbgeo; an inverted wild-type loxP site (Sauer, 1987), a promoter-less neomycin resistance gene from plasmid pMC1NeopA (Thomas and Capecchi, 1987) including a Kozak consensus sequence (Kozak, 1987) followed by two successive polyadenylation sites from the bovine growth hormone gene; a mutant loxP2272 site (Siegel et al., 2001); the previously described ClopHensor cDNA (Arosio et al., 2010) followed by the SV40 polyadenylation site, both sequences in reverse orientation relative to neomycin transcription; a wild-type loxP site and finally a mutant loxP2272 site in reverse orientation. The targeting vector was electroporated into A9 embryonic stem cells (ESC) and homologous recombinants identified by Southern blotting. Digested DNA using Bgl1 and BspHI underwent hybridization with a 3' and 5' probe, respectively and DNA fragments were visualized. A correctly identified clone was used for injection into C57BN/6 blastocysts followed by implantation of injected blastocysts into CD1 foster mothers, and backcross of male chimaeras with C57BL/6 females.

All animal protocols were approved by the Italian Ministry of Health, by the Local Ethics Committee of Kazan State Medical University (N°742.13.11.84 and N°1045-72 and by the INSERM Ethics Committee for Animal Experimentation (#30-03102012).

Brain slices

Acute hippocampal slices were obtained from 7-14 days old mice. Animals were decapitated, whole brains were rapidly removed from the skull and immersed in ice-cold solution containing (in mM) 122 Choline chloride, 2.5 KCl, 1.25 NaH_2PO_4, 25 $NaHCO_3$, 8 glucose, 0.5 $CaCl_2$ and 7 $MgCl_2$, saturated with 95% O_2 and 5% CO_2 (pH 7.3-7.4; 290-300 mOsm). Cerebral hemispheres and brainstem were separated and sliced in sagittal projection and in frontal projection, respectively. 300-µm-thick sections were prepared in the same ice-cold choline-based solution using a tissue slicer (model NVSLM1, World Precision Instruments). Before confocal imaging, slices were incubated for 1 h at room temperature in a chamber filled with oxygenated artificial cerebrospinal fluid (aCSF) containing (in mM) 126 NaCl, 3.5 KCl, 2 $CaCl_2$, 1.3 $MgCl_2$, 1.2 $NaHPO_4$, 10 glucose, 25 $NaHCO_3$ (pH 7.3-7.4, 290-300 mOsm). During recordings slices were continuously perfused with oxygenated aCSF.

Confocal fluorescence imaging of brain slices and neuro-muscular junctions

To study the localization of E^2GFP and DsRed into brain slices and presynaptic terminals of neuro-muscular junctions, the Leica SP5 TCS (Leica, Germany) laser confocal scanning microscope was used. Observations were performed using the HC X APO L 20×/1.0 W (1.00 NA) water immersion lens. The 488nm laser line was attenuated to 6% intensity and a range of 500nm - 550nm was used to detect the emitted E^2GFP. For visualization of DsRed the 561nm laser line was attenuated to 9% intensity. In this case, we detected fluorescence in the range of 600nm - 670nm. Data were analyzed using the LAS AF

Lite software on a series of "lookthrough" projections of average intensity. Brain slices were transferred to Petri dishes and placed on the microscope setup for observation. Isolated levator auris longus (LAL) nerve–muscle preparations (Angaut-Petit et al., 1987) were stretched approximately to their resting length, pinned on a Sylgard-lined Petri dish with oxygenated Krebs-Ringer solution. Krebs-Ringer solution contained the following (in mM): 135 NaCl, 5 KCl, 2 $CaCl_2$, 1 $MgCl_2$, 1 NaH2PO_4, 12 $NaHCO_3$, and 11 glucose, pH 7.2–7.4. with oxygenated (95% O2, 5%CO_2). Surface neuro-muscular junctions were located using the transmitted light channel of the confocal microscope.

Two-photon imaging

After tissue slice preparation as indicated above, the slices were transferred to the submerged chamber of the two-photon microscope setup (Femto3D-AO, Femtonics Ltd, Budapest, Hungary) and kept at 32 °C. The hippocampal CA1 area was located using the 850nm infrared LED illumination placed underneath the sample and the transmitted light was followed with a CMOS camera. After changing the light path with an automatized sliding mirror, the slices were imaged through a femtosecond laser (MaiTai HP, SpectraPhysics, Mountain View, CA, USA) set to 810nm to excite both E^2GFP and DsRed. The light path of the microscope was the same as previously described (Katona et al., 2012). Briefly, red and green fluorescence were separated by a dichroic filter (39 mm, 700dcxru, Chroma Technology) and were collected by GaAsP photomultiplier tubes custom-modified for high collection efficiency of scattered photons (PMT, H7422P-40-MOD, Hamamatsu), fixed directly onto the objective arm. The forward emitted fluorescence was also collected by 2-inch aperture detectors positioned below the condenser lens (Femto2DAlba, Femtonics). Signals of the same wavelength measured at the epi- and transfluorescent positions have been totalled. All measurements except otherwise noted were carried out using the large aperture XLUMPlanFI20x/0.95 (Olympus, 20×, NA 0.95) objective.

Measurement control, real-time data acquisition and analysis were performed with a MATLAB-based program (MES, Femtonics) and by custom-written software. The response was calculated from the raw data after manual selection of regions of interest by applying the equation:

$$\Delta G/R = (G-G_0) / R$$

where G and G_0 are the background-corrected post-stimulus and pre-stimulus green fluorescence, while R is the background-corrected red fluorescence.

Real-time fluorescence imaging

Fluorescence images were acquired using a customized digital imaging microscope. Excitation of cells at various wavelengths was achieved using a Polychrome V monochromator (Till Photonics, Germany). Light intensity was attenuated using neutral density filters. Emission wavelengths were controlled using a Lambda 10-3 controller (Sutter Instrument Company, USA). Fluorescence was visualized using an upright microscope Axioskop (Zeiss, Germany) equipped with 20x, 40x and 60x water-immersion objectives (Olympus, USA). Emitted fluorescent light was recorded through a 16-bit digital camera (Andor iXon EM+; Andor Technology PLC, Northern Ireland). Images were acquired on a computer via a DMA serial transfer. All peripheral hardware control, image acquisition and image processing were managed using the the Andor iQ software (Andor Technology PLC). The average fluorescence intensity of each region of interest (ROI) was measured.

Cells expressing ClopHensor variants were excited at three wavelengths: 458 and 488 nm for Cl^-/pH-sensitive E^2GFP excitation, and 545 nm for excitation of DsRed-monomer. Fluorescent signals were recorded using a dual-band GFP/DsRed 493/574 dichroic mirror and two emission filters: 535±15 nm for E^2GFP emission and 632±30 nm for the emission of DsRed-monomer. The emission filters were mounted into the Lambda 10-B Filter wheel (Sutter Instruments Company, Novato, USA) of the microscope.

Tissue clarification

Solutions. The following chemicals were used : paraformaldehyde (PFA, CARLO ERBA 387507-1KG), NaOH (Sigma 71687-100G), HCl (Sigma-Aldrich 258148-100ML), acrylamide (BioRad 161-0140), bis-acrylamide (BioRad 161-0142), Na_2HPO_4 dihydrate (Sigma 30435-1KG), NaH_2PO_4 (Sigma RDD007-1KG), NaCl (CARLO ERBA 479689-5KG), boric acid (Sigma B7901-5006), sodium dodecyl sulfate (SDS, Millipore 428015), Triton X-100 (Sigma T8787-250ML), sodium azide , Isoflurane (Forene), Ketamine (50 mg/mL solution), Xylazine (20 mg/mL solution).

Stock solutions: **16% PFA:** 80 g PFA was dissolved in 400 ml of DirectQ water heated to 60 °C, and 10 ml 1N NaOH were added. After the solution became clear 5 ml of 1N HCl were added, and the volume was adjusted with DirectQ to 500 ml. **10x PBS**: 0.16M Na_2HPO_4, 0.04M NaH_2PO_4 (0.2M total phosphate), 0.154M NaCl, 28.5g Na_2HPO_4 dihydrate, 4.8g NaH_2PO_4, 9g NaCl were dissolved in 800 mL of DirectQ water, the volume was then adjusted with DirectQ water to 1L. **1M boric acid, pH 8.5**: 62 g of boric acid were dissolved in 800 Ml DirectQ upon addition of 30 mL of 5N NaOH, pH was adjusted to 8.5 by 5N NaOH, and the volume was adjusted with DirectQ water to 1L; the solution was filtered through 0.22 µm PES filter (Corning 431161) and stored at 4 °C. **20% (wt/wt) SDS:** 100 g SDS were dissolved in 400 g of DirectQ water by heating; the solution was stored at room temperature. **10% Triton X-100:** 1 mL Triton X-100 was added to 9 mL of DirectQ water. **1% (wt/vol) sodium azide:** 100 mg sodium azide were dissolved in 10 mL of DirectQ water.

Working solutions: **Hydrogel solution:** 4% acrylamide, 0.05% bis-acrylamide, 0.25% wt/vol VA-044 polymerization thermoinitiator, 1x PBS, 4% PFA. 40 mL of 10x PBS, 40 mL of 40% acrylamide, 10 mL of 2% bis-acrylamide, 100 mL of 16% PFA and 1g of VA-044 were added on ice to 210 mL of DirectQ water, stirred, divided on ice into 40 mL aliquots in 50 mL centrifuge tubes and stored at -20 °C. **Clearing solution:** 0.2M boric acid, 4% (wt/vol) SDS. 400 mL of 1M boric acid and 400 mL of 20% (wt/wt) SDS were mixed with DirectQ water up to 2L. **PBST:** 1x PBS, 0.1% (vol/vol) Triton X-100. 20 mL of 10x PBS and 2 mL of 10% (vol/vol) Triton X-100 were added to 178 mL of DirectQ water. **Boric acid - Triton:** 0.2M boric acid, 0.1% (vol/vol) Triton X-100. 80 mL of 1M boric acid and 4 mL of 10% (vol/vol) Triton X-100 were added to 316 mL of DirectQ water. **PBST-azide:** 1x PBS, 0.1% (vol/vol) Triton X-100, 0.01% (wt/vol) sodium azide. 5 mL of 1% (wt/vol) sodium azide were added to 500 mL of PBST. **Ketamine-Xylazine:** 10 mg/mL Ketamine, 1 mg/ml Xylazine in 1x PBS. Sequentially 0.2 mL of 50 mg/mL Ketamine, 0.05 mL 20 mg/mL Xylazine and 0.75 mL 1x PBS were loaded into a 1 mL syringe using a needle.

16% PFA, 20% (wt/wt) SDS, 1% (wt/vol) sodium azide, the hydrogel solution and PBST-azide were all prepared in the fume hood since their components are highly toxic.

Clearing protocol. Thy1-ClopHensor 18- and 20-week old male mice were sedated by isoflurane, and the body weight was determined. Mice were then anaesthetized by intraperitoneal injection of Ketamine (100 mg kg^{-1}) and Xylazine (10 mg kg^{-1}) and transcardially perfused in the fume hood at 3 ml/min with 50 ml ice-cold 1x PBS followed by 30 ml ice-cold hydrogel solution. Brains were extracted and incubated in 40 ml of hydrogel solution at 4 °C for 3-4 days. Hydrogel solution in brain-containing centrifuge tubes was bubbled with N_2 for 5 minutes/tube using a N_2 pressure tin (Sigma-Aldrich 00474), and then allowed to polymerize during incubation in a water thermal bath at 37 °C and 28 cycles per minute for 4 hours. The excess of the polymerized hydrogel was removed.

One of the ClopHensor brains was cut in 2mm-thick coronal blocks with a single-edge razor blade using an adult mouse brain slicer matrix. Blocks were then cleared in 50 ml centrifuge tubes with 20 ml

clearing solution in a water thermal bath at 37 °C and 28 cycles per minute for one week, with the clearing solution being refreshed every 1-2 days. The cleared samples were then washed in PBST three times (for 15 minutes, overnight and for 3 hours), under the same incubation conditions as for clearing, and stored in PBST-azide.

The whole-brain hydrogel hybrids were cleared passively in 50 ml centrifuge tubes containing 40 mL of clearing solution (0.2M boric acid, 4% SDS, pH 8.5) by constant shaking in a water bath at 37 °C and 28 cycles per minute for 2 months. The clearing solution was changed every day except weekends during first 5 weeks and then every 3-4 days. After the clearing step the samples were incubated at constant shaking at 22 °C and 28 cycles per minute consequently in 40 ml of 0.2M boric acid with 0.1% (vol/vol) Triton X-100 for 2 days (the solution was refreshed after 1 day), and in 40 ml of PBST (1x PBS with 0.1% (vol/vol) Triton X-100) for 8 hours, and then stored in PBST with 0.01% (wt/vol) sodium azide. During the clearing step the samples enlarged reaching the final size of approximately 2.2x1.8x1.7 cm.

Confocal imaging of brain blocks

A custom-made chamber was built for confocal imaging (**Fig.S1,a**). For every chamber a 15 ml centrifuge tube cap was put upside-down inside a cover from a 40 mm Petri dish (50 mm in diameter), and an approximately 5-6 mm-thick sylgard layer was created between the cap and the inner wall of the cover. After the polymerization of the sylgard, the cap was removed, and the sylgard layer was extracted and flipped upside down into the same Petri dish cover. An additional portion of liquid sylgard was added between the bottom of the cover and the polymerized sylgard layer to seal hermetically the chamber. Before imaging, the clarified coronal brain blocks were incubated for 2-3 hours in the chambers filled with the X-CLARITY refraction index homogenization solution (Logos Biosystems, France) and covered with 35-mm round coverslips. After treatment the samples got completely transparent (**Fig.S1,b**). Due to the high density of X-CLARITY solution, the samples were floating just beneath the coverslip, allowing easy in-depth imaging. The brain blocks were imaged with the Olympus FV500 confocal microscope or the Zeiss LSM 510 Meta confocal microscope using 488 nm and 536 nm excitation lasers ("E^2GFP" and "DsRed" channels, respectively). The Olympus setup, in contrast to the Zeiss one, allowed full-depth imaging of the 2mm-thick blocks but was not equipped with automatic mosaic scanning and stitching, so each block was imaged using the Olympus setup in the manual mosaic mode.

Confocal image processing for the semi-quantitative fluorescence pattern analysis

After imaging, 3D-stitching of the separate block fragments was performed using a custom-written MATLAB script to reconstruct the 3D-volume of the entire blocks. For the further analysis, nine representative optical slices distributed along the rostro-caudal axis of the brain were chosen, and for each of them the corresponding Nissl-stained section from Allen Brain Institute (ABI) Mouse Brain Atlas (http://atlas.brain-map.org) was determined. The chosen stitched optical slices were manually registered into the ABI sections using the TrakEM2 plugin (Cardona et al., 2012) for Fiji (Schindelin et al., 2012) by applying non-linear transformations. The relevant ABI Atlas structure grids were downloaded from ABI's website as .svg files, and the regions of interest (ROI) corresponding to the lowest-level structures in the ABI Atlas ontology tree were determined using the 'Threshold' and 'Create Selection' function in Fiji. The ROI set was then transferred into MATLAB using the ReadImageJROI.m script from Dylan Muir (https://www.mathworks.com/matlabcentral/fileexchange/32479-readimagejroi), and further analysis was performed in MATLAB using custom-written scripts. The fragments of the fluorescent images corresponding to every ROI were determined and assigned to a brain structure according to ABI Atlas.

The structure was determined as a closed area of the ABI structure grid, or several areas having the same name. Brightness of the single structure was defined as the sum of the pixel values within the ROI divided by the area of the ROI. If the structure appeared in more than one optical section, the brightness was determined as the sum of the pixel values within the ROIs corresponding to the structure on all sections divided by the sum of the areas of the corresponding ROIs on all sections. A total of 463 structures in 9 optical sections from 8 brain blocks were analysed. Among them, 448 occupied the lowest level of the ontology tree out of 1022 lowest-level structures included in the ABI ontology. Areas corresponding to the ventricular system, and also the areas not assigned to a lowest-level structure on the current ABI section, were excluded from analysis. Lowest-level structures for which the fluorescence was quantified were then ranked according to their brightness and classified into brightest, medium and faintest 33%. Additionally, from the brightest third, 50 top-fluorescent structures were determined. The ranking and fluorescence-based structure classification were performed for left and right hemispheres separately.

Light-sheet imaging

Before imaging, samples were incubated in 87% glycerol to homogenize the refraction index for 2.5 days for ClopHensor brain samples. Just before the imaging session, the glycerol was degassed by ultrasound treatment for 20 minutes to prevent formation of multiple bubbles. The samples were imaged in 100 ml 87% glycerol with the binocular-based Ultramicroscope II light-sheet setup (LaVision BioTec, Germany) in horizontal dorso-ventral configuration, 4-step mosaic mode, and in coronal caudo-rostral configuration, 2-step mosaic mode. The light-sheet was created by converging 3 plane light rays onto the sample from either side of it. Two sets of excitation/emission filters were used, 560±40 nm / 620±60 nm ("DsRed channel"), and 470 ± 40 nm / 535 ± 30 nm ("E^2-GFP channel"). The objective working distance allowed imaging up to 1.5 cm deep.

The brain structures were identified by visual referencing of the single optical slices to the Allen Brain Institute Mouse Brain Atlas using the Brain Explorer 2 software (Allen Brain Institute, USA). Custom-written MATLAB scripts were used to annotate the structures and to construct the ontology trees by parsing the xml file of the brain ontology downloaded from the Allen Brain Institute website. Figures were prepared using Fiji (Schindelin et al, 2012) and Inkscape (Open Invention Network, LLC, USA). Imaris software (BITPLANE, UK) was used for 3D-rendering.

RESULTS

ClopHensor transgenic mice

We generated a line of transgenic mice expressing Thy1::ClopHensor using a previously described strategy (Batti et al., 2013). Preliminary imaging analyses on living tissues showed robust expression of ClopHensor in the hippocampus (Video S1), dentate gyrus (Fig. 1B) and even in the nerves from motoneurons, suggesting the possibility of monitoring Cl^-/pH transients in the presynaptic terminals of neuro-muscular junctions (Fig. 1C; Video S2).

Previous observations (Raimondo et al., 2013) indicated that the expression of ClopHensor in neurons often resulted in homogeneous E^2GFP expression, while DsRed was partially expressed heterogeneously as small intracellular aggregations (Raimondo et al., 2013). A similar tendency was observed in neurons from brain slices of our transgenic mice. (Figures 1B and 2A). These small DsRed aggregations were present mainly in neurons which morphologically looked unhealthy or dying. Surprisingly, in nerves and presynaptic terminals of neuro-muscular junctions, both E^2GFP and DsRed showed uniform fluorescence, even at high resolution (Fig. 1C, inserts for green and red fluorescence).

The investigation of the reasons for these differences in fluorescence distribution between neurons and neuro-muscular terminals was outside the scope of the present study.

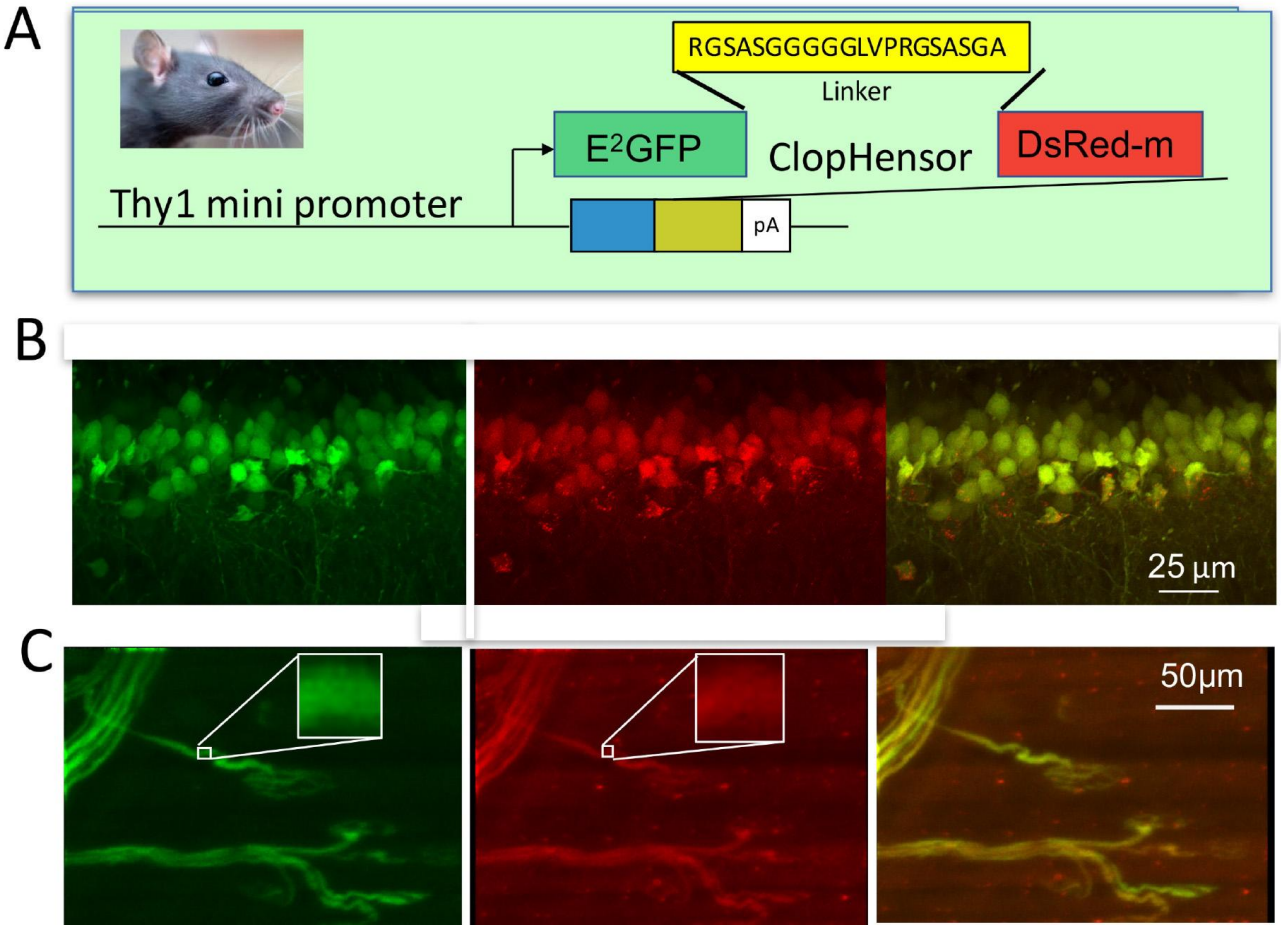

Figure 1. Expression of ClopHensor in Thy1::ClopHensor transgenic mice. (**A**) Scheme of the Thy1::ClopHensor construct. A fragment containing minimal regulatory elements derived from the promoter of the Thy1 gene is positioned upstream of the coding sequence of the ClopHensor which is followed by a SV40 polyadenylation signal. (**B**) Confocal images obtained from a coronal hippocampal brain slice, corresponding to a z-stack projection of 102 optical sections spaced 500 nm, showing neurons in the dentate granule cell layer. (**C**) Confocal images obtained from isolated neuro-muscular junctions from LAL corresponding to a maximum intensity z projection of a stack of 75 optical sections spaced 500 nm.
(**B,C**) Endogenous fluorescence of E^2 GFP (left panel), DsRed (center panel) and merged (right panel). Inserts in (C) illustrate homogenous expression of E^2GFP and DsRed (approx. 5µm^2).

The ability of ClopHensor to monitor simultaneously changes in the concentrations of Cl^- and H^+ in neurons was tested on freshly prepared hippocampal slices from transgenic mice using our customized microscope. It has been previously shown on transgenic mice expressing Cl-Sensor that the depolarization of neurons causes strong elevation of intracellular Cl- (Batti et al., 2013). To obtain a rapid depolarization of neurons in brain slices, we exploited high frequency stimulation of Shaffer collaterals. Glutamate-induced depolarization of neurons caused remarkable changes in Cl– and H+ -dependent fluorescence (Fig. 2B) indicating that ClopHensor represents a good tool for monitoring the intracellular Cl^- and H^+ transients in different neurons of transgenic mice.

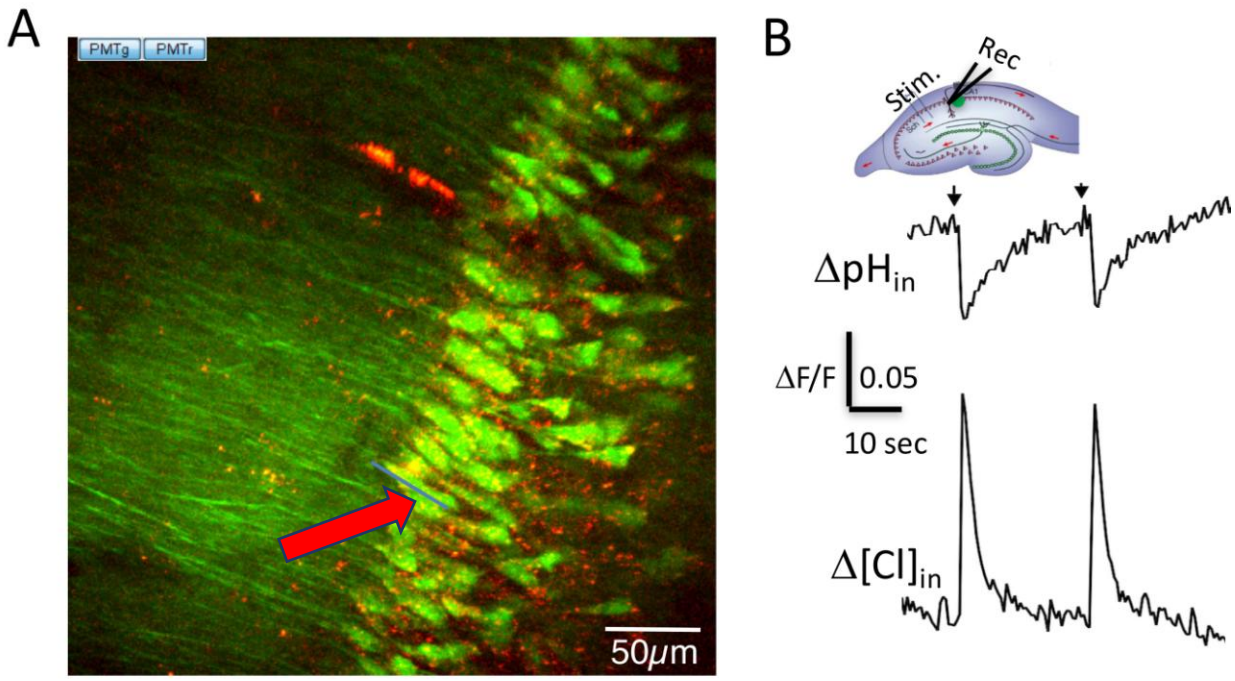

Figure 2. Fluorescence transients elicited by synaptic stimulation in the hippocampal CA1
(**A**) Two-photon imaging of ClopHensor fluorescence in the CA1 area of hippocampus. 350μm thick slice z-projection from image stack. 2P excitation wavelength: 810nm. Green detection: ~510nm; red detection: >540nm. Overlay of green and red channels. (**B**) Top panel, scheme of a hippocampal slice showing the areas of stimulation (Stim) and fluorescence recording (green ring). Bottom panel, simultaneous recording of relative changes in ΔpH_{in} (F488/F458) (top trace) and in $\Delta[Cl]_{in}$ (F458/F545) (bottom trace) after stimulation of Schaffer collaterals (100 Hz, 2sec, 120-170 μA, single pulse width 200μs). Schaffer collaterals/commissures were stimulated using the DS2A isolated stimulator (Digitimer Ltd, UK) with a bipolar tungsten electrode. Stimulus application is indicated by an arrow.

For the systematic analysis of ClopHensor expression in different parts of the brain, we used the CLARITY protocol (Tomer et al., 2014 and see Methods) to clear tissue samples and obtain transparent brains while preserving the fluorescence of the ClopHensor.

Confocal images of the ClopHensor in transparent mouse brains
Confocal imaging of eight 2mm-thick coronal ClopHensor mouse brain blocks revealed ClopHensor-expressing cells in different brain regions (**Fig. 3**). Signals from the DsRed and E^2GFP channels were perfectly colocalized (**Fig. 3A**), even though the DsRed signal was stronger, providing cell images with much better contrast. For this reason we recorded the majority of the confocal images of brain blocks in the DsRed channel only. In all ClopHensor-expressing cells we were able to image neuronal somata, and in many cases the starting portions of the protrusions were evident as well (**Fig.3B-F** and **H**, **Videos S3-S5**). 3D-rendering of the neurons in the dentate nucleus (**Video S6**) shows the organisation of the somata and their protrusions in space.

Our CLARITY protocol thus preserved ClopHensor fluorescence well enough to image neurons and, notably, their protrusions. However, the bright spots noticeable in protrusions and in some somata may indicate slight protein clusterisation that might result from fixation or polymerization or reflect some inherent property of DsRed (Sacchetti et al., 2002; Raimondo et al., 2013).

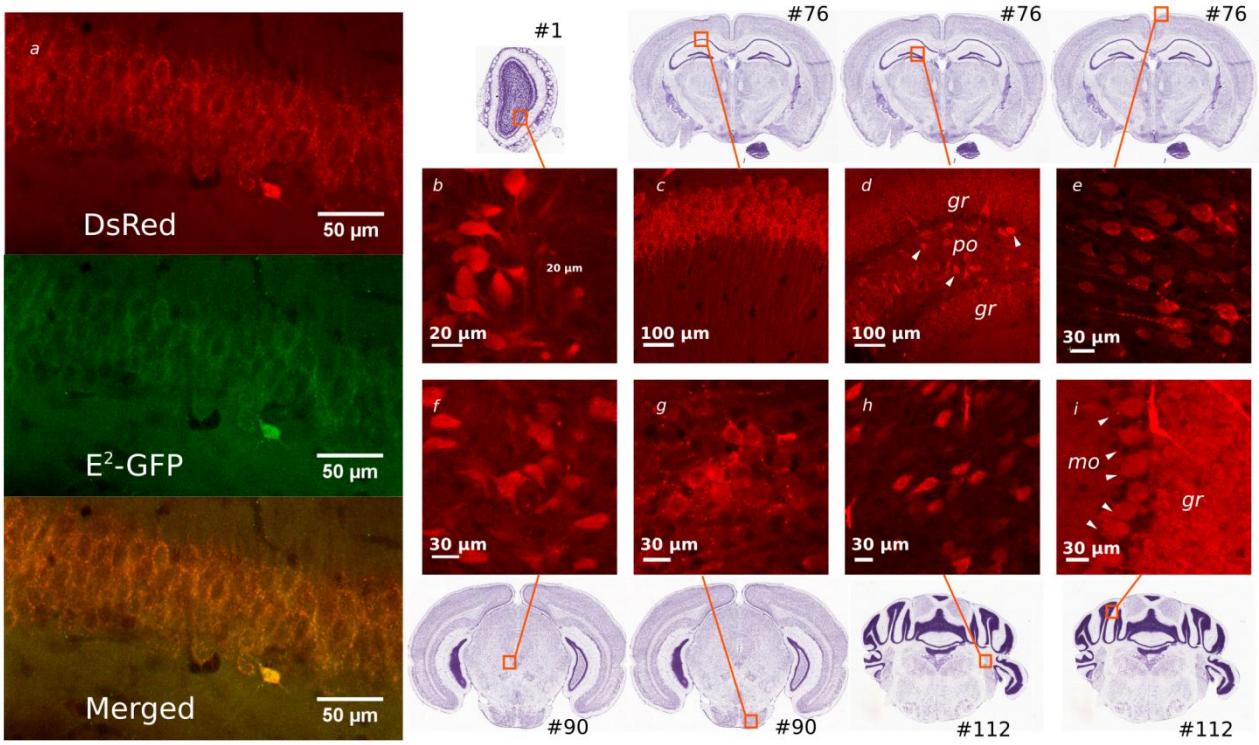

Figure 3. Confocal images of clarified ClopHensor mouse brain 2mm-thick blocks. (**A**) ClopHensor-expressing neurons in the entorhinal area imaged in the DsRed (excitation at 536 nm) and E^2GFP (excitation at 488 nm) channels. The merged image provides evidence for the colocalization of the two signals. (**B-I**) ClopHensor-expressing cells in different brain regions imaged in the DsRed channel: (**B**), olfactory bulb, mitral layer*;* (**C**), CA1 field, pyramidal layer; (**D**), dentate gyrus, granular and polymorph layers (arrows indicate mossy cells); (**E**), retrosplenial area of the isocortex, layer 5; (**F**), oculomotor nucleus in the midbrain; (**G**), pontine gray; (**H**), dentate nucleus; (**I**), cerebellar lobule (arrows indicate Purkinje cells). Nissl-stained sections from the Allen Brain Institute Mouse Brain Atlas with the locations of the cells in (**B-I**) are shown above or below. The number of the section of ABI Atlas is provided for every section. *mo*, molecular layer; *gr*, granular layer, *po*, polymorph layer.

Expression pattern of ClopHensor revealed by light-sheet microscopy

Combination of two caudo-rostral and four dorso-ventral imaging series covered almost the whole clarified brain sample (**Fig. 4,a-h** and **Videos S7-S8**). Imaged regions include the isocortex below the level of the dorsal part of the retrosplenial area; olfactory areas caudal to the nucleus of the lateral olfactory tract, except the frontal parts of the olfactory bulbs not preserved upon brain extraction; the hippocampal formation; the cortical subplate; the striatum above the anterior area of the amygdala; the pallidum above the magnocellular nucleus; the thalamus; the hypothalamus above the supraoptic nucleus; the midbrain; the pons; the medulla rostral to the nucleus ambiguus; and the cerebellum.

Similarly to confocal microscopy, the fluorescence in the DsRed channel was much brighter than the one in the E^2-GFP channel, and we thus performed the analysis using only the data from the DsRed channel. Quantitative description of the light-sheet data is complicated due to the inherently imperfect distribution of the exciting light intensity over the optical slice and to potential inhomogeneities of the transparency within the sample. To estimate qualitatively the ClopHensor expression pattern, we categorized the structures that are fluorescent in the DsRed channel into two categories, with lower and higher fluorescence, respectively (Groups 1 and 2). Only structures in the left hemisphere were considered.

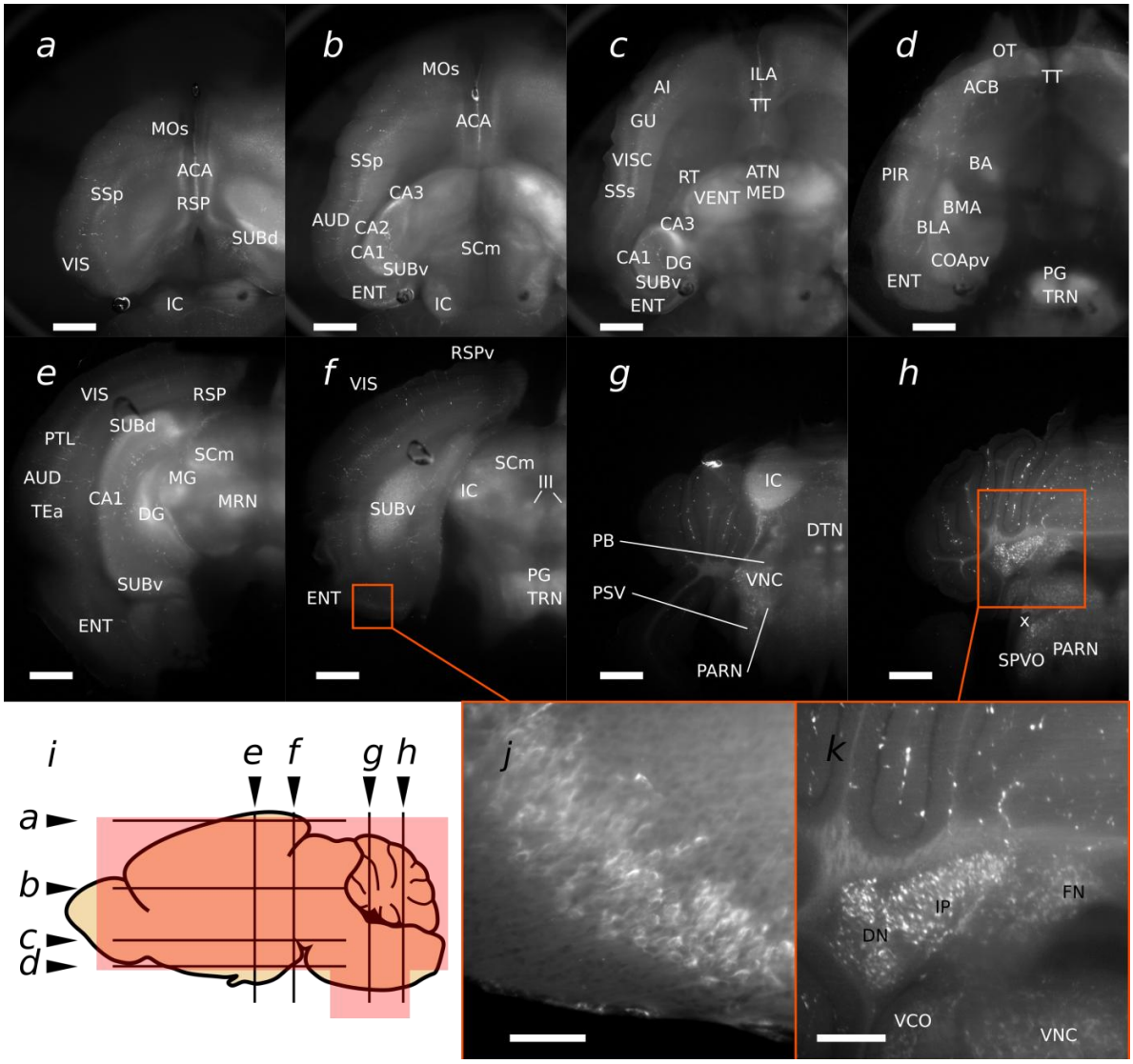

Figure 4. Light-sheet microscopy imaging of the clarified ClopHensor mouse brain in the DsRed channel (excitation at 560±40 nm, emission filtered at 620±40 nm). (**A-D**) horizontal, and (**E-H**) coronal optical sections at 1.6x. The position of the sections and the overall imaged regions (transparent red area) are shown in (**I**). (**J**) ClopHensor-expressing neurons in the entorhinal area at 12.6x. (**K**) zoomed image of the cerebellar nuclei at 1.6x. Scale bars: (**A-H**) 2 mm; (**J**), 100 µm; (**K**), 600 µm. The brightest structures are annotated using ABI acronyms (**Table 1**).

Acronyms of the brain structures used throughout the present study are listed in **Table 1**. Acronyms of the structures from the Groups 1 and 2 are listed in **Table 2**, and the combined ontology tree is presented in **Table S1**, with Group 2 structures highlighted in bold. The ontology tree of the structures not imaged through light-sheet microscopy is shown in **Table S2**.

In the isocortex, layer 5 was fluorescent in the majority of the inspected fields, with the ventral part of the retrosplenial area and the somatosensory areas being the brightest. DsRed fluorescence could be observed in the somatosensory, gustatory, visceral, auditory, anterior cingulate areas and the ventral part of the retrosplenial area in both layers 2/3 and 5. In the frontal pole, primary motor, perirhinal and entorhinal areas the fluorescence was not appreciable or much less pronounced. In the hippocampal formation, the brightest fields included the stratum oriens and the pyramidal layer of

CA1 and CA2, the stratum lucidum of CA3, the dorsal and ventral parts of the subiculum and the entorhinal area. In the thalamus, the highest DsRed fluorescence corresponded to the ventral, anterior and medial group of the dorsal thalamus, as well as the reticular nucleus of the thalamus. The central and external nuclei of the inferior colliculus represented the brightest regions of the midbrain. In the pons, the brightest fluorescence was observed in the tegmental reticular nucleus and in the pontine gray. The medulla showed fluorescence in the majority of its structures with the external cuneate, parvicellular reticular and vestibular nuclei and the spinal nucleus of the trigeminal being the brightest. Additionally, the three cerebellar nuclei (dentate, interposed and fastigial) were also very fluorescent.

3D-rendering of the dorso-ventral imaging series (**Video S9**) revealed that the highest levels of DsRed fluorescence pertained to the isocortex, Ammon's horn, the subiculum, the inferior colliculus, the tegmental reticular nucleus and the pontine gray.

The specificity of the DsRed signal observed in light-sheet imaging is confirmed by the observation of single fluorescent cells either at low magnification, for example, in the cerebellar nuclei (**Fig. 4K** and **Video S7**) or at higher magnification, for example, in the entorhinal area (**Fig. 4J** and **Video S10**) and in the anterior cingulate area (**Video S11**).

Semi-quantitative analysis of ClopHensor expression pattern using confocal microscopy

Since the light-sheet images can be analysed only qualitatively, we attempted to quantify the stitched confocal images of 9 representative optical sections from 8 brain blocks (**Fig.5**).

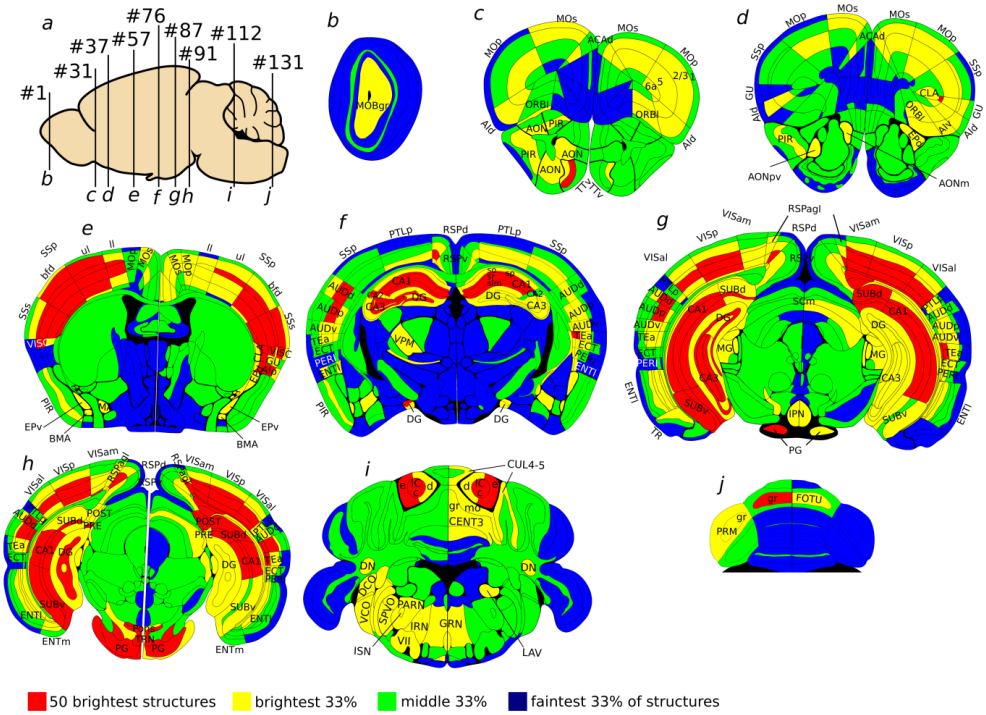

Figure 5. Semi-quantitative analysis of the ClopHensor expression pattern based on confocal data. (**A**) Scheme indicating the positions of the 9 optical sections chosen for the analysis, and the numbers of the corresponding sections from the ABI Mouse Brain Atlas. (**B-J**) ABI Mouse Brain Atlas structure grids corresponding to the 9 analysed confocal optical sections, showing lowest-level structures ranked according to their brightness. ABI acronyms (**Table 1**) are used for annotation. Only those grey-substance structures in which at least 1 layer belongs to the brightest 33% have been annotated. Black areas represent either the ventricular system or areas not assigned to a lowest-level structure on the corresponding ABI section.

The chosen sections, after stitching and overlaying with the corresponding ABI structure grids, are shown in **Fig. S2**. The list of acronyms in **Table 2** and the ontology tree in **Table S3** show the 33%

brightest structures among all the analysed left-hemisphere structures, wherein the 50 brightest structures are highlighted in bold. The 50 brightest structures roughly corresponded to the Group 2 structures identified through light-sheet imaging (**Table 2**). They included layers in the visual, auditory, gustatory, somatosensory, visceral, retrosplenial, temporal association and agranular insular areas of the isocortex; the ventral taenia tecta; fields CA1-3 of the dentate gyrus, the pre- and post-subiculum and the subiculum; the central and external nuclei of the inferior colliculus; the tegmental reticular nucleus and the pontine gray; the granular layer of folium-tuber vermis (VII).

The brightest 33% structures in the left hemisphere included, in addition to the ones mentioned above, the motor, anterior cingular, orbital, ecto- and perirhinal areas of the isocortex; the granular layer of the olfactory bulb, the anterior olfactory and piriform nuclei, the postpiriform transition area; entorhinal areas; the endopiriform nucleus; the medial geniculate complex and some nuclei of the ventral group of the dorsal thalamus; the motor related area of the superior colliculus, the interpeduncular nucleus; the dentate nucleus; and some lobuli of the cerebellum.

The ontology tree of the left-hemisphere structures with intermediates levels of fluorescence (middle 33%) is reported in **Table S4**. These structures included, besides some cortical layers, the mitral layer of the main olfactory bulb, the dorsal taenia tecta, the dorsal peduncular area, discrete regions of the cortical amygdala and of the postpiriform transition area; specific layers of the entorhinal area in the hippocampal formation; the claustrum and parts of the endopiriform and basolateral amigdalar nuclei in the cortical subplate; certain regions of the striatum and the pallidum, several sensory-motor and polymodal association cortex related areas of thalamus and large areas in the midbrain, hindbrain, cerebellar cortex and many fiber tracts.

Table S5 shows the ontology tree of the set of structures not included in the analysis of the confocal images.

The proposed semi-quantitative analysis appeared to reliably define large expression areas but was less sensitive to particular layers. Thus, for the majority of the areas of the isocortex any layer may be listed as fluorescent (Tables 2 and S3-S4). However, visual inspection of confocal images confirmed that the fluorescence is constrained to the layers 2/3 and 5 (**Fig. S3**) of the isocortex.

DISCUSSION

In this study, we present a novel line of transgenic mice expressing ClopHensor and provide a detailed map of its distribution in the mouse brain. Compared to transient viral gene transfer, the development of transgenic mice provides stable long-term expression and importantly allows systematic analyses in multiple animals characterized by identical expression patterns of the genetically encoded sensor.

Previously, we have generated two transgenic mouse lines expressing a CFP-YFP-based Cl^- probe called Cl-Sensor either under the control of a Thy1 mini promoter, or via Cre-mediated recombination in the Rosa26 locus (Batti et al., 2013). These mouse lines demonstrated high levels of tissue-specific expression in neurons, particularly, in the cortex and hippocampus, and in peripheral sensory neurons. Using simultaneous whole-cell monitoring of ionic currents and fluorescence analysis in brain slices and cell culture, the Cl-Sensor was calibrated and reliable non-invasive recordings indicated that these mouse lines represent useful models for monitoring of intracellular Cl^- in specific cell types. However, Cl-Sensor exhibits also a relatively high sensitivity to pH variations (Markova et al., 2008; Batti et al., 2013; Raimondo et al., 2013).

This issue has been solved by creating ClopHensor, a biosensor which allows simultaneous monitoring of intracellular Cl^- and H^+ concentrations (Arosio at al., 2010). This construct consists of a Cl^- -and pH -sensitive GFP mutant, E^2GFP, and monomeric DsRed, linked by a flexible 20-amino-acid spacer. The functional properties and the calibration of ClopHensor after expression in cell lines were

described previously (Mukhtarov et al, 2013) and in the present study we present transgenic mice expressing ClopHensor under the neuronal Thy1 promoter. Preliminary recordings on brain slices show that glutamate-induced depolarization caused by stimulation of Schaffer collaterals resulted in strong changes of fluorescence in hippocampal neurons expressing ClopHensor.

To determine the *in vivo* pattern of ClopHensor expression, adult mouse brains have been cleared using the passive CLARITY technique (Tomer et al., 2014; Yang *et al.* ,2014). Confocal and light-sheet microscopy analyses of the distribution pattern and approximate intensity of ClopHensor fluorescence allowed us to generate a detailed map of its expression in the whole mouse brain.

Similarly to other Thy1 transgenic mice, ChlopHensor mice show mosaic expression, with variable distribution and intensity across different brain regions. Among the 50 brightest structures, in addition to hippocampus, particularly high levels of expression were detected in the visual, auditory and somatosensory areas and in several thalamic, midbrain and cerebellar nuclei. Areas with lower levels of expression, including the midbrain, hindbrain and the cerebellar cortex can still be used for fluorescent monitoring. In addition, ClopHensor is highly expressed in axons of motoneurons and in nerve terminals. Its expression is strong and homogeneous over millimeter-long distances, which is important for reliable analysis of ion transients in axons and neuro-muscular junctions.

Altogether our results report a detailed map of ClopHensor distribution in the mouse brain, providing a way for the non-invasive monitoring of Cl^- and H^+ concentrations in multiple neuronal subsets, moroneurons and nerve terminals in different experimental models and over long periods of the animal's life.

Acknowledgements

We are grateful to Drs. I. Medina, F. Michel and F. Magdinier for their help with confocal and light-sheet monitory recordings and analysis, to Drs. G. Maleeva, A. Ivanov, M.Mitchel and A. Ghestem for their help with PCR analysis and performing some experiments. We are grateful to FRC Kazan Scientific Center of RAS for providing some experimental equipment.

Funding:

AD was financed by by Mechnikov Bursary-2016 from the French Embassy in Moscow. This work was supported by the Russian Science Foundation (grant number: 18-15-00313 for PB and EP) ERA SynBIO grant MODULIGHTOR (PCIN-2015-163-C02-01 for PB). AK was financed by EC Marie Curie Intra-European Fellowship (ImagINE, grant agreement No 625372). FZ and CTG were supported by funds from EMBL

Conflict of interest

The authors declare that there are no conflicts of interest.

Role of authors:

A.D. performed all Clarity experiments, analysis, data interpretation and writing the MS; D.S., A.K., A.M., E.P. and M.E. contributed to performing different experiments and to the drafting; C.G., F.Z., A.C., D.A. - transgenic mice developing; P.B. - designing the project, data interpretation, analysis and writing the MS.

TABLES

Table 1. ABI acronyms used for the brain structures

Isocortex: **MOp**, primary motor area; **MOs**, secondary motor area; **SSp**, primary somatosensory area: **bfd**, barrel field, **ul**, upper limb, **ll**, lower limb; **SSs**, supplemental somatosensory area; **GU**, gustatory areas; **VISC**, visceral area; **AUD**, auditory areas; **AUDp**, primary auditory area; **AUDd**, dorsal auditory area; **AUDv**, ventral auditory area; **AUDpo**, posterior auditory area; **VIS**, visual areas; **VISp**, primary visual area; **VISal**, anterolateral visual area; **VISl**, lateral visual area; **VISpl**, posterolateral visual area; **VISam**, anteromedial visual area; **VISpm**, posteromedial visual area; **ACAd**, anterior cingulate area, dorsal part; **ACAv**, anterior cingulate area, ventral part; **ILA**, infralimbic area**; ORBm**, orbital area, medial part; **ORBl**, orbital area, lateral part; **AI**, agranular insular area; **AId**, agranular insular area, dorsal part; **AIv**, agranular insular area, ventral part; **AIp**, agranular insular area, posterior part; **RSPd**, retrosplenial area, dorsal part; **RSPv**, retrosplenial area, ventral part; **RSPagl**, retrosplenial area, lateral agranular part; **PTLp**, posterior parietal association areas; **TEa**, temporal association areas; **ECT**, ectorhinal area; **PERI**, perirhinal area. **Olfactory areas:** **MOBmi**, granule layer of the main olfactory bulbs**; MOBgr**, granule layer of the main olfactory bulbs; **AON**, anterior olfactory nucleus; **AONd**, anterior olfactory nucleus, dorsal part**; AONpv**, anterior olfactory nucleus, posteroventral part; **AONm**, anterior olfactory nucleus, medial part**; TT**, taenia tecta**; TTd**, taenia tecta, dorsal part; **TTv**, taenia tecta, ventral part; **PIR**, piriform area: **PIR1**, molecular layer, **PIR2**, pyramidal layer, **PIR3**, polymorph layer; **COAp**, cortical amygdalar area, posterior part; **TR**, postpiriform transition area. **Hippocampal formation:** **CA1**, field CA1, **CA2**, field CA2, **CA3**, field CA3: **slm**, stratum lacunosum-moleculare, **so**, stratum oriens, **sr**, stratum radiatum, **slm**, stratum lacunosum-moleculare, **sp**, pyramidal layer, **slu**, stratum lucidum; **DG**, dentate gyrus: **DG-po**, polymorph	**Cortical subplate:** **CLA**, claustrum; **EP**, endopiriform nucleus; **EPd**, endopiriform nucleus, dorsal part; **EPv**, endopiriform nucleus, ventral part; **LA**, lateral amygdalar nucleus; **BLA**, basolateral amygdalar nucleus; **BMA**, basomedial amygdalar nucleus: **BMAa**, anterior part, **BMAp**, posterior part; **PA**, posterior amygdalar nucleus. **Cerebral nuclei:** **OT**, olfactory tubercle; **ACB**, nucleus accumbens; **BA**, bed nucleus of the accessory olfactory tract; **MA**, magnocellular nucleus. **Thalamus:** **VENT**, ventral group of the dorsal thalamus; **VPM**, ventral posteromedial nucleus of the thalamus; **MG**, medial geniculate complex: **MGd**, dorsal part, **MGv**, ventral part; **LGd**, dorsal part of the lateral geniculate complex; **LAT**, lateral group of the dorsal thalamus: **SGN**, suprageniculate nucleus; **ATN**, anterior group of the dorsal thalamus; **MED**, medial group of the dorsal thalamus; **PVT**, paraventricular nucleus of the thalamus; **CL**, central lateral nucleus of the thalamus; **PF**, parafascicular nucleus; **RT**, reticular nucleus of the thalamus. **Hypothalamus:** **SBPV**, subparaventricular zone; **MBO**, mammillary body; **LHA**, lateral hypothalamic area; **LPO**, lateral preoptic area. **Midbrain:** **IC**, inferior colliculus: **ICe**, external nucleus, **ICc**, central nucleus, **ICd**, dorsal nucleus; **NB**, nucleus of the brachium of the inferior colliculus; **MEV**, midbrain trigeminal nucleus; **RR**, midbrain reticular nucleus, retrorubral area; **MRN**, midbrain reticular nucleus; **SCm**, superior colliculus, motor related; **CUN**, cuneiform nucleus; **RN**, red nucleus; **III**, oculomotor nucleus; **SNc**, substantia nigra, compact part; **PPN**, pedunculopontine nucleus; **IPN**, interpeduncular nucleus. **Pons:** **NLL**, nucleus of the lateral lemniscus**; PSV**, principal sensory nucleus of the trigeminal; **PB**, parabrachial nucleus; **DTN**, dorsal tegmental nucleus; **PCG**, pontine central gray; **PG**, pontine gray;	**Medulla:** **CNlam**, granular lamina of the cochlear nuclei**; DCO**, dorsal cochlear nucleus; **VCO**, ventral cochlear nucleus; **ECU**, external cuneate nucleus; **NTS**, nucleus of the solitary tract; **SPVI**, spinal nucleus of the trigeminal, interpolar part; **SPVO**, spinal nucleus of the trigeminal, oral part: **SPVOrdm**, rostral dorsomedial part, **SPVOvl**, ventrolateral part;; **ISN**, inferior salivatory nucleus; **VI**, abducens nucleus; **VII**, fascial motor nucleus; **ACVII**, accessory facial motor nucleus; **GRN**, gigantocellular reticular nucleus; **IRN**, intermediate reticular nucleus; **ISN**, inferior salivatory nucleus; **LRN**, lateral reticular nucleus; **MARN**, magnocellular reticular nucleus; **PARN**, parvicellular reticular nucleus; **PGRN**, paragigantocellular reticular nucleus; **PRP**, nucleus prepositus; **VNC**, vestibular nuclei; **LAV**, lateral vestibular nucleus; **MV**, medial vestibular nucleus; **SUV**, superior vestibular nucleus; **x**, nucleus x; **RM**, nucleus raphe magnus. **Cerebellar cortex:** **CENT3**, Lobule III; **CUL4-5**, Lobule IV-V; **PRM**, paramedian lobule: **PRMmo**, molecular layer, PRMgr, granular layer; **FOTU**, folium-tuber vermis (VII): **FOTUgr**, granular layer. **Cerebellar nuclei:** **FN**, fastigial nucleus; **IP**, interposed nucleus; **DN**, dentate nucleus. **fiber tracts:** **arb**, arbor vitae; **bsc**, brachium of the superior colliculus; **sptV**, spinal tract of the trigeminal nerve; **vVIIIn**, vestibular nerve; **tb**, trapezoid body; **bic**, brachium of the inferior colliculus; **ml**, medial lemniscus; **mcp**, middle cerebellar peduncle; **icp**, inferior cerebellar peduncle; **cst**, corticospinal tract; **alv**, alveus.

layer, **DG-sg**, granule cell layer, **DG-mo**, molecular layer; **ENT**, entorhinal area; **ENTl**, entorhinal area, lateral part; **ENTm**, entorhinal area, medial part; **PAR**, parasubiculum; **POST**, postsubiculum; **PRE**, presubiculum; **SUBd**, subiculum, dorsal part: **SUBd-m**, molecular layer, **SUBd-sp**, pyramidal layer, **SUBd-sr**, stratum radiatum; **SUBv**, subiculum, ventral part: **SUBv-m**, molecular layer, **SUBv-sp**, pyramidal layer, **SUBv-sr**, stratum radiatum.	**PRNc**, pontine reticular nucleus, caudal part; **SG**, supragenual nucleus; **TRN**, tegmental reticular nucleus; **V**, motor nucleus of trigeminal; **LC**, locus ceruleus; **PRNr**, pontine reticular nucleus.	

Table 2. Left-hemisphere structures fluorescent in DsRed channel on confocal and light-sheet images. The digits after the acronyms define the layers inside the structures.

Light-sheet (Group 2 shown in bold)	Confocal (brightest 33%). In bold, are shown 50 brightest structures.
Isocortex: MOs5, **SSp2/3, SSp5, SSs2/3, SSs5, GU2/3, GU5, VISC2/3, VISC5**, **AUDd2/3, AUDd5, AUDp2/3, AUDp5, AUDpo2/3, AUDpo5, AUDv2/3, AUDv5**, VISal2/3, VISal5, VISl2/3, VISl5, **VISp2/3, VISp5, VISpl5, VISpm5**, **ACAd2/3, ACAd5, ACAv2/3, ACAv5, PL5, ILA5**, ORBm5, AIp2/3, AIp5, AIv2/3, AIv5, **RSPv2/3, RSPv5,** PTLp5, TEa5 **Olfactory areas:** MOBmi, MOBgr, **TTd2, TTv2**, PIR1, PIR2, PIR3, **COAp**, TR3 **Hippocampal formation: CA1so, CA1sp**, **CA2so, CA2sp**, **CA3slu,** CA3so, **DG-po, DG-sg**, **ENTl5, ENTm1, ENTm2,** PAR2, POST2, PRE2, **SUBd-sp, SUBv-sp** **Cortical subplate:** EP, LA, **BLA, BMA,** PA **Cerebral nuclei: OT, ACB**, **BA** **Thalamus: VENT**, MG, LGd, LAT, **ATN, MED,** PVT, CL, PF, **RT** **Hypothalamus:** SBPV, MBO, LHA, LPO **Midbrain: ICc,** ICd, **ICe,** NB, MEV, RR, MRN, SCm, CUN, RN, III, SNc, PPN **Pons:** NLL, **PSV,** PB, **DTN,** PCG, **PG,** PRNc, SG, **TRN, V**, LC, PRNr **Medulla:** DCO, VCO, **ECU,** NTS, **SPVI, SPVO**, VI, VII, ACVII, GRN, IRN, ISN, LRN, MARN, **PARN,** PGRN, PRP**,** LAV, MV, SUV, **x**, RM **Cerebellar nuclei: FN, IP, DN** **fiber tracts:** arb	**Isocortex:** MOp5, MOs1, MOs2/3, SSp-bfd1, **SSp-bfd2/3, SSp-bfd4, SSp-bfd5, SSp-bfd6a, SSp-bfd6b,** SSp-ll2/3, **SSp-ll4, SSp-ll5,** SSp-ll6a, **SSp-ul2/3, SSp-ul4, SSp-ul5, SSp-ul6a,** SSp-ul6b, SSs2/3, **SSs4, SSs5, SSs6a, SSs6b, VISC4, VISC5,** VISC6a, AUDd2/3, **AUDd4, AUDd5, AUDp5,** AUDp6a, AUDpo4, **AUDpo5, AUDpo6a, AUDpo6b,** AUDv4, AUDv5, AUDv6a, VISal2/3, VISal4, **VISal5,** VISal6a, VISal6b, VISam4, VISam5, VISam6a, VISam6b, VISp2/3, **VISp4, VISp5, VISp6a,** VISp6b, ACAd5, ORBl1, AId2/3, AId5, RSPagl2/3, RSPagl5, RSPagl6a, RSPagl6b, RSPd5, **RSPd6a,** RSPd6b, RSPv6a, RSPv6b, PTLp6a, TEa4, TEa5, TEa6a **Olfactory areas:** MOBgr, AONd, AONm, AONpv, **TTv2,** TTv3, PIR2, TR3 **Hippocampal formation: CA1slm,** CA1so, **CA1sp, CA1sr,** CA2slm, **CA2so, CA2sp,** CA2sr, **CA3slm,** CA3slu, CA3so, **CA3sp, CA3sr,** DG-mo, DG-po, **DG-sg,** ENTl2/3, ENTl3, ENTl4, ENTl5, ENTl6a, ENTl6b, ENTm2, ENTm3, ENTm5, ENTm6, POST1, POST2, POST3, **PRE1,** PRE2, SUBd-m, SUBd-sp, **SUBd-sr, SUBv-m, SUBv-sp, SUBv-sr** **Cortical subplate:** EPv, BMAa, BMAp **Cerebral nuclei:** MA **Thalamus:** VPM, MGd, MGv, SGN **Midbrain: ICc,** ICd, **ICe,** IPN **Pons: PG, TRN** **Medulla:** CNlam, DCO, VCO, SPVOrdm, SPVOvl, VII, GRN, IRN, ISN, PARN, RM **Cerebellar cortex: FOTUgr,** PRMmo, PRMgr **Cerebellar nuclei:** DN **fiber tracts:** bsc, sptV, vVIIIn, tb, bic, ml, **mcp,** icp, **cst,** alv

Figure legends.

Figure 1. Expression of ClopHensor in Thy1::ClopHensor transgenic mice. (**A**) The scheme of Thy1::ClopHensor construct. A fragment containing minimal regulatory elements was fused with the promoter of the Thy1 gene upstream to the coding sequence of the ClopHensor followed by a SV40 polyadenylation signal. (**B**) Confocal image obtained from a coronal hippocampal brain slice, corresponding to a z-stack projection of 102 optical slices spaced at 500 nm, showing neurons in the dentate granule cell layer. (**C**) Confocal image obtained from isolated neuro-muscular junction from LAL corresponding to a maximum intensity z projection of a stack of 75 optical slices spaced at 500 nm. (**B,C**) shows endogenous fluorescence of E^2 GFP (left), DsRed (center) and merged (right). *Inserts in **C***: about 5µm square illustrating homogenous expression of E^2GFP and DsRed.

Figure 2. Fluorescence transients elicited by synaptic stimulation in the hippocampal CA1
A, Two-photon monitoring of ClopHensor fluorescence in CA1 area of hippocampus. 350µm thick slice z-projection from image stack. 2P excitation wavelength: 810nm. Green detection: ~510nm; red detection: >540nm. Overlay of green and red channels. B, top, Scheme of hippocampal slice showing the areas of stimulation (Stim) and fluorescence monitoring (green ring). B, bottom, Simultaneous recording of relative changes in ΔpH_{in} (F488/F458) (top trace) and in $\Delta[Cl]_{in}$ (F458/F545) (bottom trace) after stimulation of Schaffer collaterals (100 Hz, 2sec, 120-170 µA, single pulse width 200µs). Schaffer collateral/commissures were stimulated using the DS2A isolated stimulator (Digitimer Ltd, UK) with a bipolar tungsten electrode. The moments of stimuli application are indicated by arrows.

Figure 3. Confocal images of the clarified ClopHensor mouse brain 2mm-thick blocks. *a*, ClopHensor-expressing neurons in the entorhinal area imaged in DsRed (excitation at 536 nm) and E^2GFP (excitation at 488 nm) channels; the merged image provides evidence for the colocalization of the two signals. *b-i*, ClopHensor-expressing cells in different brain regions imaged at 536 nm excitation: *b*, olfactory bulb, mitral layer; *c*, CA1 field, pyramidal layer; *d*, dentate gyrus, granular and polymorph layers (arrows indicate mossy cells); *e*, retrosplenial area of the isocortex, layer 5; *f*, oculomotor nucleus in the midbrain; *g*, pontine gray; *h*, dentate nucleus; *i*, cerebellar lobule (arrows indicate Purkinje cells). Nissl-stained sections from the Allen Brain Institute Mouse Brain Atlas with the locations of the cells in *b-i* are shown above or below. The number of the section of ABI Atlas is provided for every section. *mo*, molecular layer; *gr*, granular layer, *po*, polymorph layer.

Figure 4. Light-sheet microscopy assessment of the clarified ClopHensor mouse brain in the DsRed channel (excitation at 560±40 nm, emission filtered at 620±40 nm). ***a-d***, horizontal, and ***e-h***, coronal optical sections at 1.6x. The positions of the sections and the overall imaged regions (transparent red area) are shown in ***i***. ***j***, ClopHensor-expressing neurons in the entorhinal area at 12.6x. ***k***, zoomed image of the cerebellar nuclei at 1.6x. Scale bars: ***a-h***; ***j***, 100 µm; *k,* 600 µm. The brightest structures are annotated using ABI acronyms (**Table 1**).

Figure 5. Semi-quantitative analysis of the ClopHensor expression pattern based on confocal data. ***a***, positions of the 9 optical sections chosen for the analysis, and the numbers of the corresponding sections from ABI Mouse Brain Atlas. ***b-c***, ABI Mouse Brain Atlas structure grids corresponding to the 9 analysed confocal optical sections, showing lowest-level structures ranked according to their brightness. ABI acronyms (**Table 1**) are used for annotation. For the sake of clarity only those grey-substance structures are annotated in which at least 1 layer belongs to the brightest 33%. Black areas represent either ventricular system or areas not assigned to a lowest-level structure on the current ABI section.

REFERENCES.

Angaut-Petit, D., Molgo, J., Connold, A. L., and Faille, L. (1987). The levator auris longus muscle of the mouse: a convenient preparation for studies of short-and long-term presynaptic effects of drugs or toxins. Neuroscience letters, 82(1), 83-88.

Arosio D, Ricci F, Marchetti L, Gualdani R, Albertazzi L, Beltram F. Simultaneous intracellular chloride and pH measurements using a GFP-based sensor. Nat Methods. 2010; 7(7):516-8.

Arosio, D., and Ratto, G. M. (2014). Twenty years of fluorescence imaging of intracellular chloride. Frontiers in cellular neuroscience, 8, 258.

Aslanova U.F., Morimoto T., Farajov E.I., Kumagai N., Nishino M., Sugawara N., Ohsaga A., Maruyama Y., Tsuchiya S., Takahashi S., Kondo Y. Chloride-dependent intracellular pH regulation via extracellular calcium sensing receptor in the medullary thick ascending limb of the mouse kidney. Tohoku J. Exp. Med. 2006; 210(4): 291-300.

Batti L, Mukhtarov M, Audero E, Ivanov A, Paolicelli RC, Zurborg S, Gross C, Bregestovski P, Heppenstall PA. Transgenic mouse lines for non-invasive ratiometric monitoring of intracellular chloride. Front. Mol. Neurosci. 2013; 6:11.

Berglund, K., Schleich, W., Krieger, P., Loo, L. S., Wang, D., Cant, N. B., Feng, G., Augustine, G. J., and Kuner, T. (2006). Imaging synaptic inhibition in transgenic mice expressing the chloride indicator, Clomeleon. Brain Cell. Biol. 35, 207–228.

Bregestovski P., Arosio D. (2011). Green fluorescent protein-based chloride ion sensors for in vivo imaging, in Fluorescent Proteins II, Springer Ser Fluoresc, ed, Jung G., editor. (Berlin, Heidelberg: Springer-Verlag), 12, 99–124

Bregestovski P., Waseem T., Mukhtarov M. Genetically encoded optical sensors for monitoring of intracellular chloride and chloride-selective channel activity. Front. Mol. Neurosci. Dec. 2009; 2(15): 1-13.

Cardona, A., Saalfeld, S., Schindelin, J., Arganda-Carreras, I., Preibisch, S., Longair, M., ... & Douglas, R. J. (2012). TrakEM2 software for neural circuit reconstruction. PloS one, 7(6), e38011.

Caroni, P. (1997). Overexpression of growth-associated proteins in the neurons of adult transgenic mice. Journal of neuroscience methods, 71(1), 3-9.

Chung K, Deisseroth K. CLARITY for mapping the nervous system. Nat Methods. 2013; 10(6):508-13.

Dana, H., Novak, O., Guardado-Montesino, M., Fransen, J. W., Hu, A., Borghuis, B. G., ... & Svoboda, K. (2018). Thy1 transgenic mice expressing the red fluorescent calcium indicator jRGECO1a for neuronal population imaging in vivo. PloS one, 13(10), e0205444.

Feng, G., Mellor, R.H., Bernstein, M., Keller-Peck, C., Nguyen, Q.T., Wallace, M., Nerbonne, J.M., Lichtman, J.W. and Sanes, J.R., 2000. Imaging neuronal subsets in transgenic mice expressing multiple spectral variants of GFP. Neuron, 28(1), pp.41-51.

Jentsch T.J., Stein V., Weinreich F., Zdebik A.A. Molecular structure and physiological function of chloride channels. Physiol. Rev. 2002; 82(2): 503-568.

Katona, G., Szalay, G., Maák, P., Kaszás, A., Veress, M., Hillier, D., ... & Rózsa, B. (2012). Fast two-photon in vivo imaging with three-dimensional random-access scanning in large tissue volumes. Nature methods, 9(2), 201.

Kozak, M. (1987). At least six nucleotides preceding the AUG initiator codon enhance translation in mammalian cells. J. Mol. Biol. 196, 947–950.

Kuner T, Augustine GJ. A genetically encoded ratiometric indicator for chloride: capturing chloride transients in cultured hippocampal neurons. Neuron. 2000; 27(3):447-59
Markova O., Mukhtarov M., Real E., Jacob Y., Bregestovski P. Genetically encoded chloride indicator with improved sensitivity. J. Neurosci. Methods. 2008; 170(1): 67-76.
Markova, O., Mukhtarov, M., Real, E., Jacob, Y., & Bregestovski, P. (2008). Genetically encoded chloride indicator with improved sensitivity. Journal of neuroscience methods, 170(1), 67-76.
Mukhtarov M, Liguori L, Waseem T, Rocca F, Buldakova S, Arosio D, Bregestovski P. Calibration and functional analysis of three genetically encoded Cl(-)/pH sensors. Front Mol Neurosci. 2013; 6:9.
Pasantes-Morales H., Lezama R.A., Ramos-Mandujano G., Tuz K.L. Mechanisms of cell volume regulation in hypo-osmolality. Am. J. Med. 2006; 119: S4-11.
Raimondo, J. V., Joyce, B., Kay, L., Schlagheck, T., Newey, S. E., Srinivas, S., & Akerman, C. J. (2013). A genetically-encoded chloride and pH sensor for dissociating ion dynamics in the nervous system. Frontiers in cellular neuroscience, 7, 202.
Sacchetti, A., Subramaniam, V., Jovin, T. M., & Alberti, S. (2002). Oligomerization of DsRed is required for the generation of a functional red fluorescent chromophore. FEBS letters, 525(1-3), 13-19.
Sauer, B. (1987). Functional expres- sion of the cre-lox site-specific recombination system in the yeast Saccharomyces cerevisiae. Mol. Cell Biol. 7, 2087–2096.
Schindelin, J., Arganda-Carreras, I., Frise, E., Kaynig, V., Longair, M., Pietzsch, T., ... & Tinevez, J. Y. (2012). Fiji: an open-source platform for biological-image analysis. Nature methods, 9(7), 676.
Siegel, R. W., Jain, R., and Bradbury, A. (2001). Using an in vivo phagemid system to identify non-compatible loxP sequences. FEBS Lett. 505, 467–473.
Stefaniuk, M., Gualda, E.J., Pawlowska, M., Legutko, D., Matryba, P., Koza, P., Konopka, W., Owczarek, D., Wawrzyniak, M., Loza-Alvarez, P. and Kaczmarek, L., 2016. Light-sheet microscopy imaging of a whole cleared rat brain with Thy1-GFP transgene. Scientific reports, 6, p.srep28209.
Suzuki M., Morita, T., Iwamoto, T. Diversity of Cl– Channels. Cell. Mol. Life Sci. 2006; 63: 12–24.
Thomas, K. R., and Capecchi, M. R. (1987). Site-directed mutagen- esis by gene targeting in mouse embryo-derived stem cells. Cell 51, 503–512.
Tomer R, Ye L, Hsueh B, Deisseroth K. Advanced CLARITY for rapid and high-resolution imaging of intact tissues. Nat Protoc. 2014; 9(7):1682-97.
Waseem T, Mukhtarov M, Buldakova S, Medina I, Bregestovski P. Genetically encoded Cl-Sensor as a tool for monitoring of Cl-dependent processes in small neuronal compartments. J Neurosci Methods. 2010; 193(1):14-23.
Yang, B., Treweek, J. B., Kulkarni, R. P., Deverman, B. E., Chen, C. K., Lubeck, E., ... & Gradinaru, V. (2014). Single-cell phenotyping within transparent intact tissue through whole-body clearing. Cell, 158(4), 945-958.